Chapter 6. **Experimental and numerical evidence**

This chapter confirms and further analyzes the experimental evidence of asymmetric bistable flow at WiSt laboratory, by a cross-checked investigation at CRIACIV wind tunnel and numerical simulations.

6.1 CRIACIV wind tunnel (University of Florence)

6.1.1 Characteristics and instrumentation

The CRIACIV laboratory (Centro di Ricerca Interuniversitario Aerodinamica delle Costruzioni e Ingegneria del Vento, www.criaciv.unifi.it) is an open-circuit wind tunnel located at Polo Universitario Città di Prato, which is a branch of the University of Florence. The total length is about 22 m. The tunnel itself has a length of 11 m, with a slightly divergent shape from the inlet (in order to guarantee a constant pressure along the x-axis) and a test section of 2.4 m in width and 1.6 m in height. A turntable in the test section allows to test different wind directions, if necessary. A honeycomb grid is located at the inlet of the tunnel. Details of the wind tunnel are reported in the Drawing 4 on page 194).

The motor – with a nominal power of 160 kW – and the fan are placed at the end of the wind tunnel, followed by a T-shaped symmetric diffuser. The engine allows to attain a maximum wind speed of about 30 m/s with 1500 rounds per minute of the fan. The variation of the rpm is controlled through an inverter up to 50 Hz. The air flow can also be regulated by adjusting the pitch angle of the ten blades of the fan between 7.7 and 15.4. The experiments in this work are performed by setting the frequency of the inverter at either 45 Hz or 50 Hz and the pitch angle at 15.4.

The atmospheric boundary layer profile which is used in these experiments is produced by three bigger “shark-fins” and four smaller spires, followed by roughness panels with wooden cubes (Figure 6.7).

The Prandtl tube allows to measure the static and the dynamic pressure of the incoming flow. During the experiments, only one Prandtl tube, placed above the tower, has been used during pressure measurements on the model. For specific purposes, for example the measurement of the efflux velocity or the mean wind profile at the tower position, a second Prandtl tube is introduced. For the acquisition of these signals, the instruments are connected to a pressure transducer (Setra System, model 239). The

signal is then converted by 32-bit NI card and acquired by a PC. A sampling frequency of 500 Hz is used in the experiments with the Setra System.

Figure 6.1 CRIACIV wind tunnel (University of Florence)

The mean wind profile at the tower position was measured during the experiments by using a mobile Prandtl tube. The mean wind velocity has been indirectly calculated from the dynamic pressure, by using Bernoulli equation. The variation of air density due to temperature variation during the experiments is considered. The result, with respect to the velocity at the main Prandtl tube, is plotted in Figure 6.2. In fact, in order to evaluate pressure coefficients from pressure measurements, the velocity pressure itself, and not the velocity, is used in the calculation.

The turbulence intensity and integral length scale of turbulence L_{ux} were previously measured and tabulated in an internal report of the laboratory. Those data, resulting from hot-wire measurements (Figure 6.3 and Figure 6.4) are referred to in this work.

The pressures on the tower are measured using two different types of pressure scanners:

- Type 1: PSI 8400, consisting of four acquisition units having 16 piezoelectric transducers each and two acquisition units having 32 transducers each. A total

amount of 128 pressures can be recorded simultaneously at a sampling frequency of 250 Hz[4] and a time duration of 30 s.

- Type 2: DTC-Initium, two acquisition units having 32 piezoelectric transducers each. A total amount of 64 pressures can be recorded simultaneously at a sampling frequency of 500 Hz.

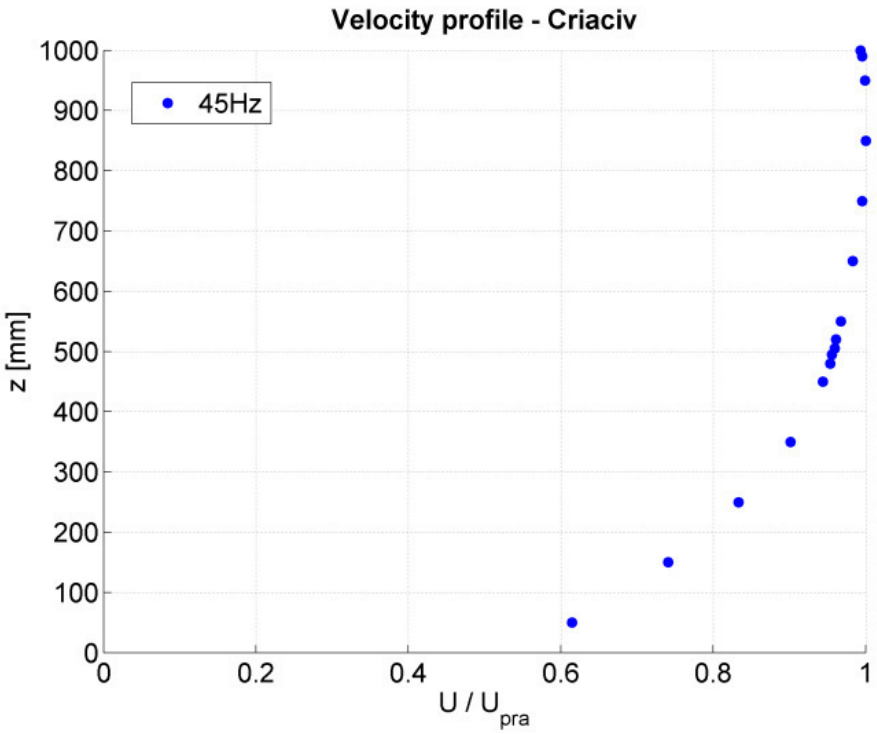

Figure 6.2 Mean wind profile

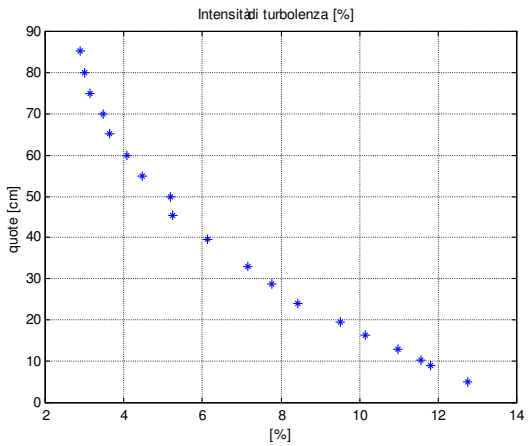

Figure 6.3 Turbulence Intensity Iu (%). (Procino, 2010)

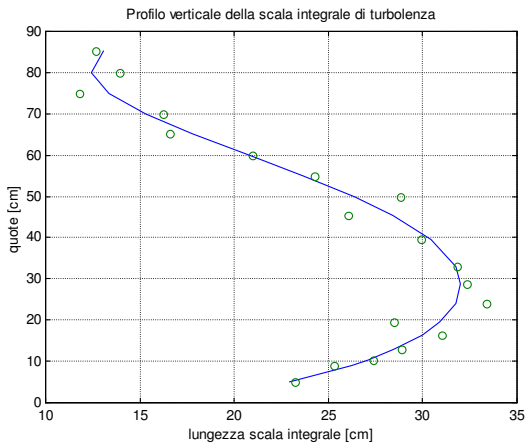

Figure 6.4 Integral length scale L_{ux} (cm). (Procino, 2010)

[4] Pressures can be measured with a sampling frequency up to 1 kHz, but the sampling frequency is inversely proportional to the number of channels which are used at the same time. if the maximum number of channels (128) is used simultaneously, the sampling frequency decreases to 250 Hz.

6.1.2 **Outline of the experiments**

The first purpose of CRIACIV experiments is to confirm the experimental evidence at WiSt laboratory, concerning the bistable and asymmetric flow. In every wind tunnel, it is absolutely common to have some disturbance in the flow. The comparison of results in the two wind tunnels proves that the occurrence of the bistable flow is not induced by some local distortion of a certain laboratory. Furthermore, the wind tunnel tests at CRIACIV allowed to better investigate the bistable flow, also at lower levels.

The two different types of pressure scanners cannot be combined together, therefore the tests are divided into two sets: one with 64 sensor type 2, distributed on three external levels in each measurements, able to measure for a relatively long time (131 s) at high sampling frequency, i.e. 500 Hz; one with 128 sensors type 1, distributed at several levels and able to measure at 250 Hz for a duration of 30 s. The set n.2 aims to attain a global correlation field, but with lower degree of detail.

The tests are repeated by using two wind tunnel velocities: $U_{pra} \approx 28$ m/s (frequency of the wind tunnel inverter = 45 Hz) and $U_{pra} \approx 30$ m/s (frequency of the wind tunnel inverter = 50 Hz). The Reynolds number are: $Re = 2.8*10^5$, $Re = 3.0*10^5$. The first one is more comparable with WiSt; the second one is a further test at a slightly higher Re, but it did not show any additional relevant feature. Therefore, the main study has been based on $Re = 2.8*10^5$.

The following series of measurements, associated to the measure of circumferential levels or vertical lines, are defined. Some of the 128 sensors type 1 were out of use at the time of the measurements. The internal pressures were measured, too, in some of the free channels.

- MS51: levels z = 990-950-910 mm;
- MS52: levels z = 910-890-850 mm;
- MS53: levels z = 850-750-650 mm;
- MS54: levels z = 650-550-520 mm;
- MS55: levels z = 520-505-495 mm;
- MS56: levels z = 495-480-450 mm;
- MS57: levels z = 450-350-250 mm;
- MS58: levels z = 250-150-50 mm;
- MS59: verticals at 0°, 20°, 40°;
- MS60: verticals at 60°, 80°, 100°;
- MS61: verticals at 120°, 140°, 160°;
- MS62: verticals at 180°, 200°, 220°;

- MS63: verticals at 240°, 260°, 280°;
- MS64: verticals at 300°, 320°, 340°;
- MS65: levels z = 950-850-750-650-550(only 9 taps)-450(only 9 taps)-50 mm;
- MS67: levels z = 950-850-750-650-550-450-350-250-150-50 mm (only 9 taps at each level);

The experimental campaign was articulated in the following two sets:

Set n.1 (March 2012):

Pressure scanners	type 2
Turbulence setting:	T5
Rings:	SR1
Efflux:	EF0/EF1
Surface roughness:	R1
Wind tunnel velocity (Hz):	45/50
Measurement series:	MS51/52/53/54/55/56/57/58/59/60/61/62/63/64;

Set n.2 (April 2012):

Pressure scanners	type 1
Turbulence setting:	T5
Rings:	SR0/SR1/SR5/SR7
Efflux:	EF0/EF1
Surface roughness:	R1
Wind tunnel velocity (Hz):	45/50
Measurement series:	MS65/67.

The efflux inside the tower is calibrated at a velocity about one half of U_{pra} (Figure 6.5). In order to adapt the model to the facilities of the laboratory, it was decided to simplify the installation (Drawing 3 on page 126, at WiSt) and remove the ventilator. In fact, a suitable opening below the model was enough to guarantee the proper efflux capacity and velocity (Figure 6.8).
However, as previously explained, the most interesting results referred to the condition without efflux.

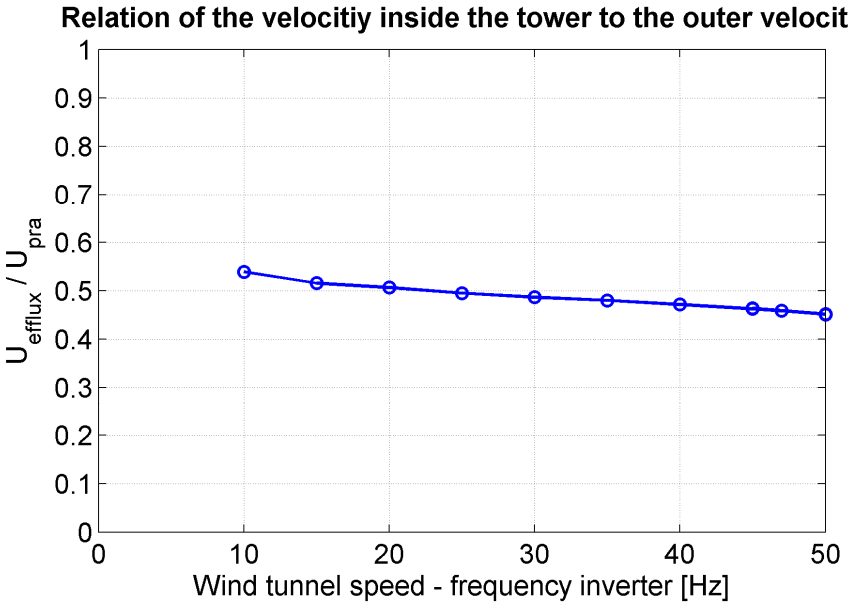

Figure 6.5 Efflux velocity

The model for the experiments is the same as in Bochum. A picture of it in CRIACIV wind tunnel is reported below (Figure 6.6). The smooth collector roof was not placed during these tests. In fact, it was seen that its presence did not affect significantly the substance of the results.

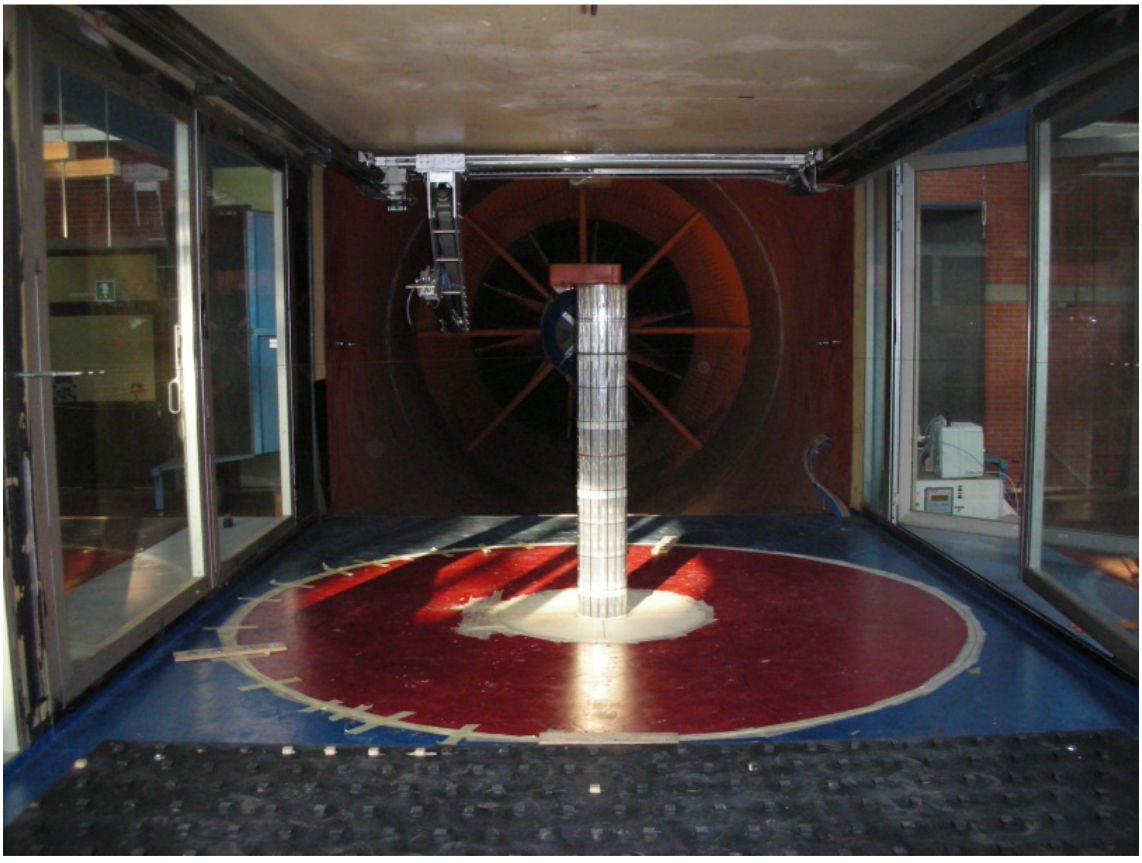

Figure 6.6 Solar tower at CRIACIV wind tunnel

Figure 6.7 Atmospheric boundary layer facilities at CRIACIV

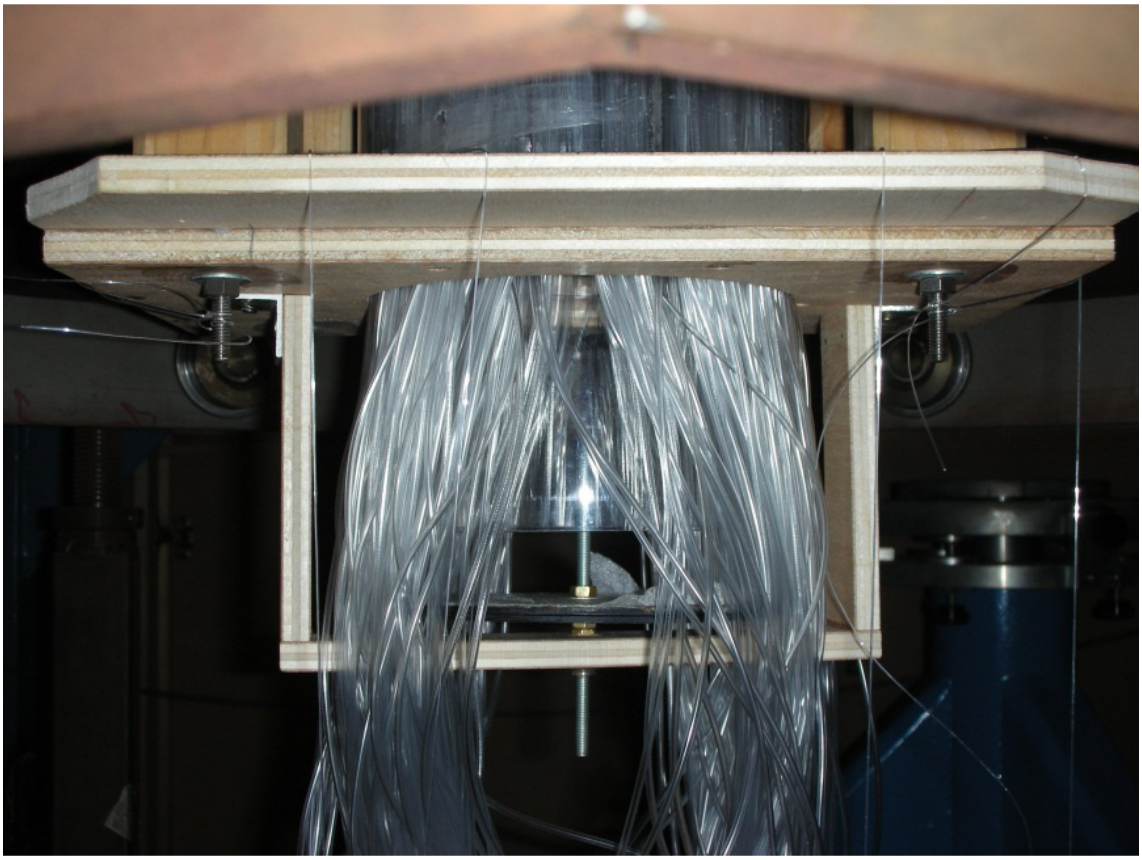

Figure 6.8 Opening below the model for creation of the efflux

DRAWING n.4 **CRIACIV Boundary layer wind tunnel University of Florence - PLAN** 0 1000 2000mm

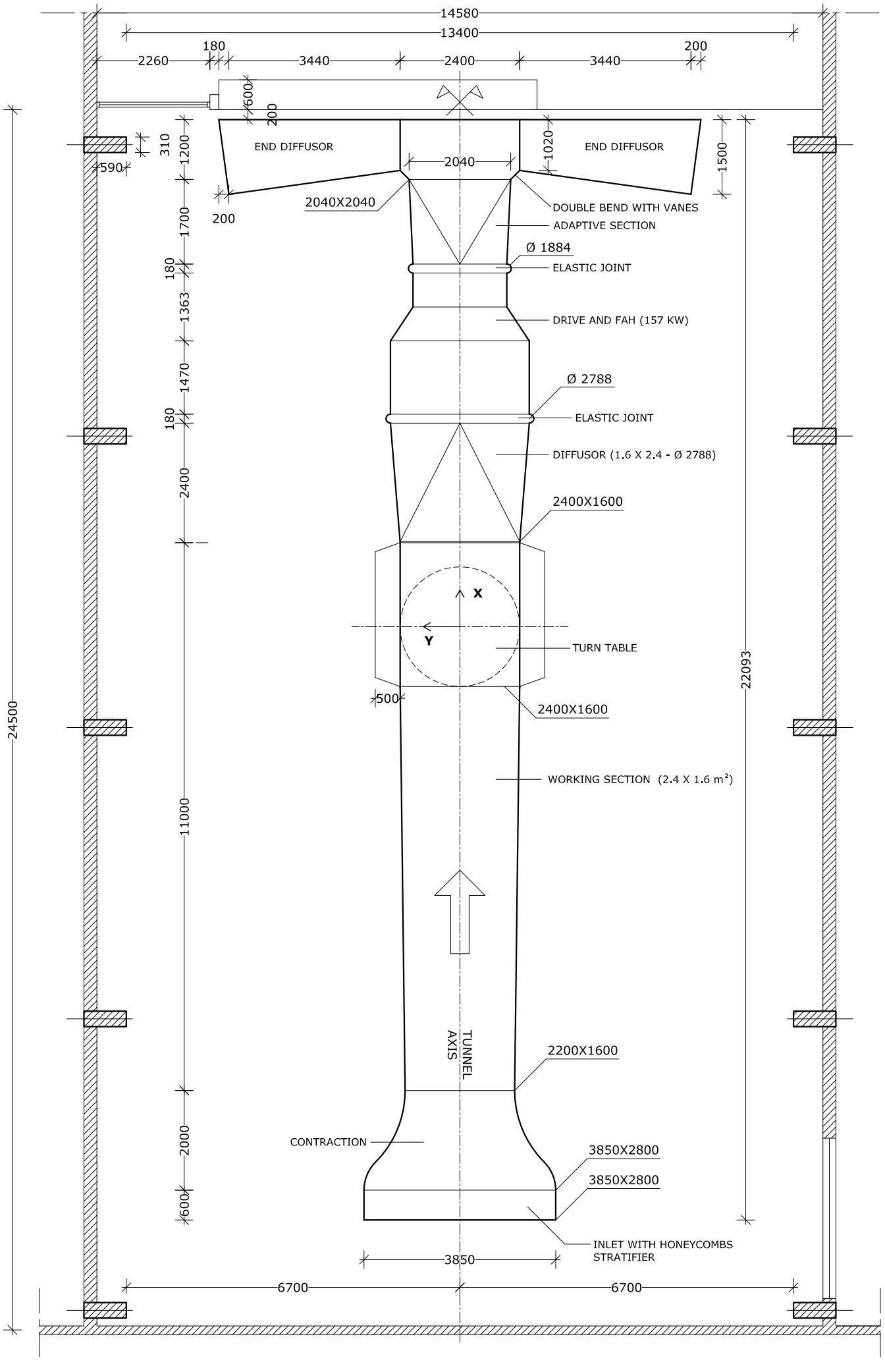

6.2 The bistable flow at CRIACIV

The wind tunnel tests at CRIACIV prove that the bistable flow is a fundamental physical phenomenon, which is not induced by some local distortion of the flow in a given laboratory. Figure 6.9 shows the comparison of pressure coefficients at 100° and at different levels along the height of the tower in the two wind tunnels, in case of ten rings along the height (SR1). The model is the same, therefore any difference between results is only attributable to the flow.

At first sight, it can be seen that the standard deviation of the time histories in each state is different at WiSt and CRIACIV, but this is not surprising, because of the different I_u. The corresponding values of I_u are reported in Table 6.1. Apart from that, the jumps occur in the same manner in the two wind tunnels.

By looking at the time histories, another evidence in the tip region is the existence, in the two wind tunnels, of a predominant state. This lasts longer in every time history. At WiSt, the predominant state in the highest compartment is state 1, i.e. the one which is characterized by positive mean lift in the reference system of the wind tunnel (Drawing 4, page 194). Being the x-axis in the along wind direction, the positive lift in the state 1 is created by a separation bubble on the 180°-360° side of the cylinder. At CRIACIV, the situation is reversed and the predominant state in the highest compartment is state 2, i.e. the one which is characterized by negative mean lift. It means that at CRIACIV the separation bubble in the highest compartment preferably develops on the 0°-180° side, instead of 180°-360° as in WiSt. Then, along the height, the inversion proceeds according to the top condition. In any case, the existence of a predominant state is not due to model imperfections, but to the flow. The question arises about what should be expected in ideal conditions. These cannot be perfectly reproduced in any experiment, but they can be reasonably assumed in a CFD simulation (this issue is addressed in section 6.4).

At a certain level along the height a sort of disruption of the bistable flow starts. The jumps between the two states become more rapid on one side of the cylinder, so that the actual state of the flow is a mixture between the two states. A further insight in this phenomenon will be discussed at the end of this section by using the histograms of pressures along the height until the very low levels. The disruption of the bistable flow starts on the high-suction side of the cylinder, i.e. on the bubble side. This is confirmed in the two wind tunnels by looking in Figure 6.9 at C_p(650mm,100°) in WiSt and C_p(750mm, 100°) in CRIACIV: those pressure taps lie, during the predominant state, on the bubble side. Figure 6.12 clarifies better what occurs at CRIACIV at the levels of disruption on the two sides of the cylinder. It can be seen that the normal side (NS)

remains unaffected until a lower level. This explains why the mixture in C_p(750mm, 260°) and C_p(650mm, 100°) in Figure 6.12 is not so evident. In fact, at those levels the separation bubble preferably develop on the other side of the cylinder, as confirmed by C_p(750mm, 100°) and C_p(650mm, 260°). There, instead, the disruption is clear because those pressure taps lie, during the predominant state, on the bubble side.

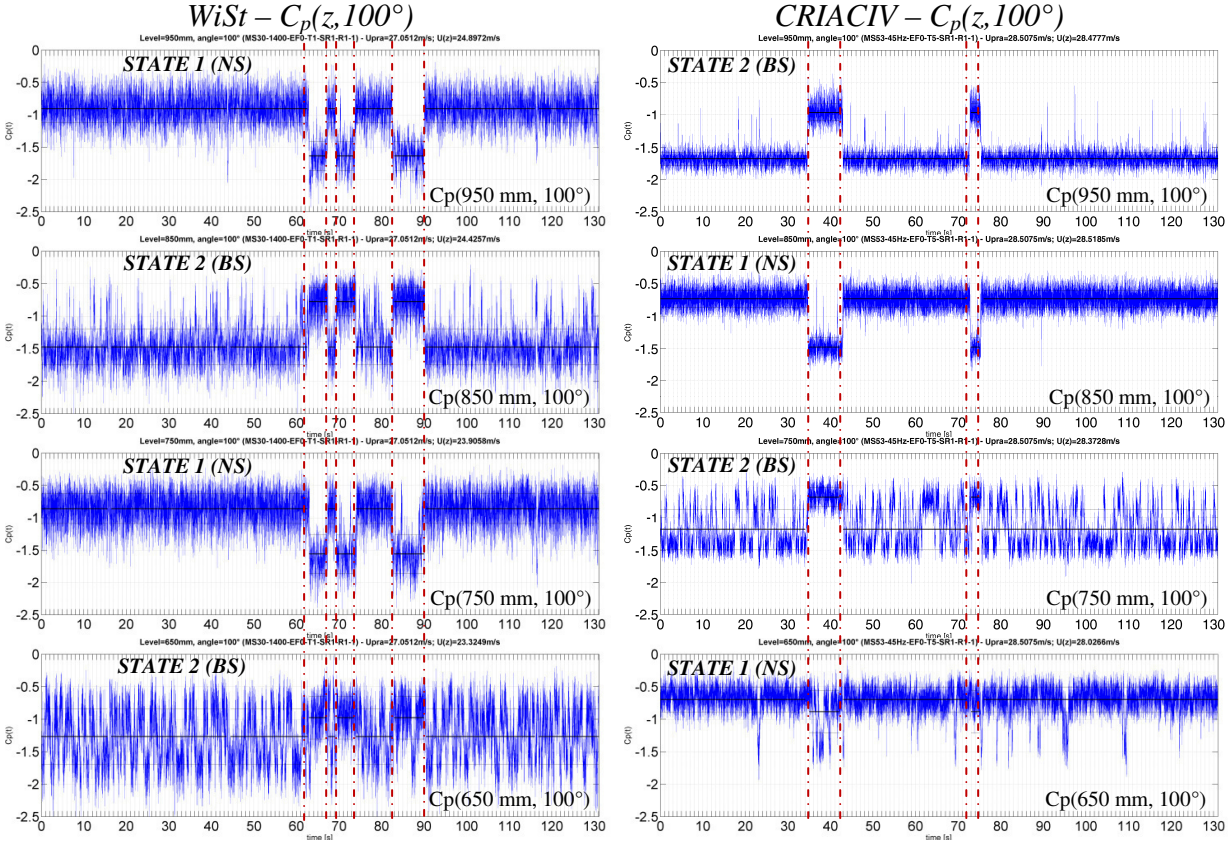

Figure 6.9 The validating result: Wist&CRIACIV (T1/T5-SR1-EF0-R1)
*NS = normal side; BS = bubble side (Re = 2.5*10^5 at WiSt, Re = 2.8*10^{5}at CRIACIV)*

Table 6.1 Turbulence intensity at WiSt and CRIACIV

z [mm]	I_u at WiSt	I_u at CRIACIV
950	0.0794	0.0283
850	0.0823	0.0283
750	0.0863	0.0309
650	0.0925	0.0359

The level at which the bistable flow starts disrupting is different in WiSt and CRIACIV. In particular, at WiSt it starts at 650 mm, while at CRIACIV it starts one compartment above, i.e. at 750 mm. This is not related to I_u, because the value of I_u at

CRIACIV at 750 mm is much lower than the I_u at WiSt, even in the highest compartment (Table 6.1). However, this must be related to the type of atmospheric boundary layer, as it is further proved at WiSt, through the tests in uniform flow (namely T3), shown in Figure 6.13. The figure plots the time histories at levels 550 and 450 mm. The equivalency between the two states is not exactly fulfilled at those levels, but it can be seen that the disruption of the bistable flow, i.e. the more rapid alternation of the two states, starts at level 450 mm on the bubble side. In uniform flow (T3) this happens two compartments lower than in atmospheric boundary layer flow (T1), in the same wind tunnel. Therefore, the spanwise development of the bistable flow must be influenced by the type of atmospheric boundary layer. However, so far it has not been identified a certain property of the boundary layer which is univocally related to the disruption of the bistable flow at a certain level.

The equivalency of the two states, in terms of mean and rms values of the pressure coefficients, is shown in Figure 6.10 and Figure 6.11 (at z = 750 mm), which are comparable to Figure 5.5 and Figure 5.6 at WiSt, respectively.

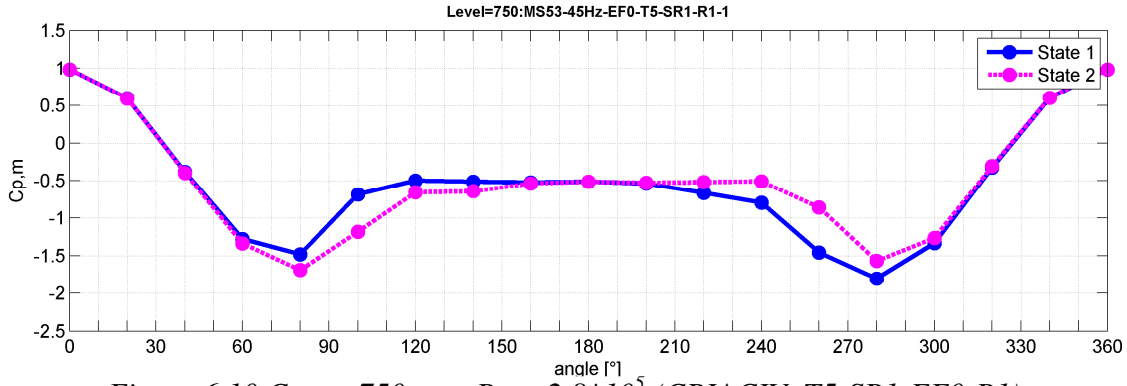

*Figure 6.10 $C_{p,m}$ at 750 mm, Re = 2.8*10^5 (CRIACIV, T5-SR1-EF0-R1) to be compared with Figure 5.5*

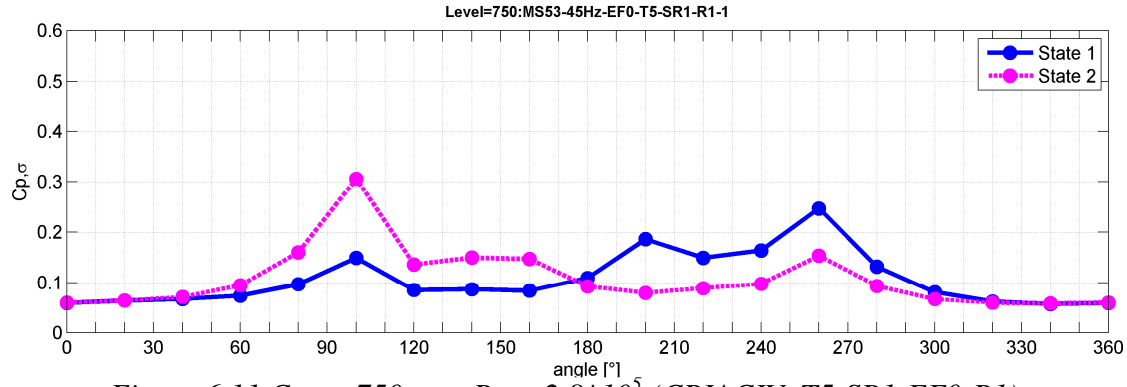

*Figure 6.11 $C_{p,\sigma}$ at 750 mm, Re = 2.8*10^5 (CRIACIV, T5-SR1-EF0-R1) To be compared with Figure 5.6*

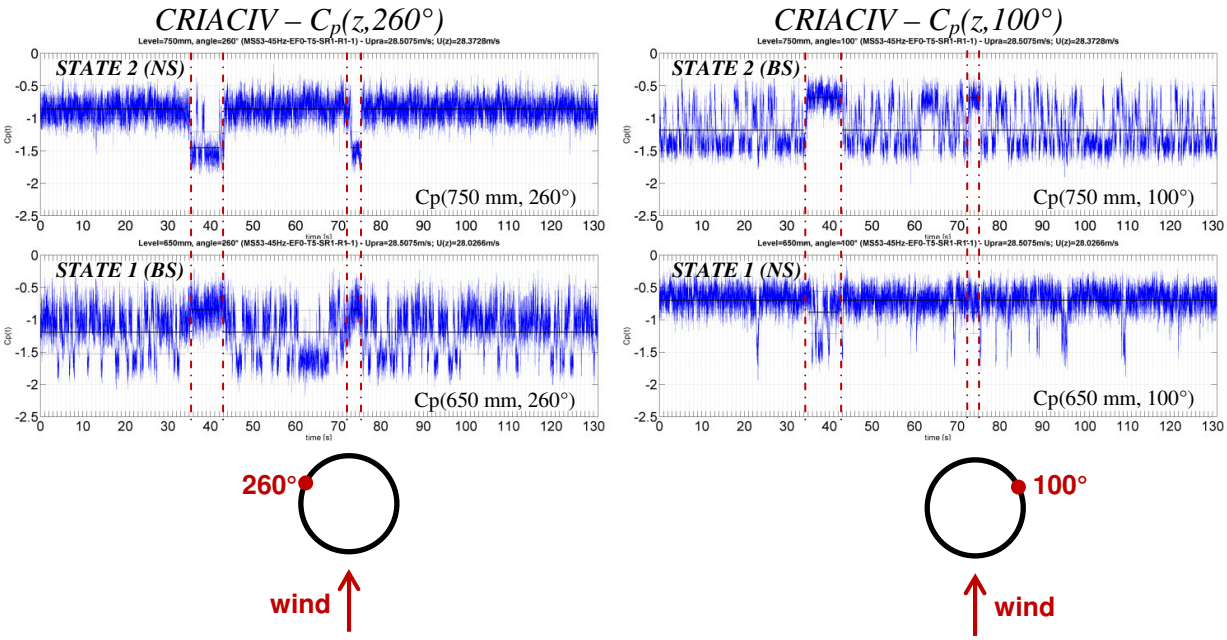

Figure 6.12 The levels of disruption (CRIACIV, T5-SR1-EF0-R1)
*NS = normal side; BS = bubble side (Re = 2.8*10^5, z = 650, 750 mm)*

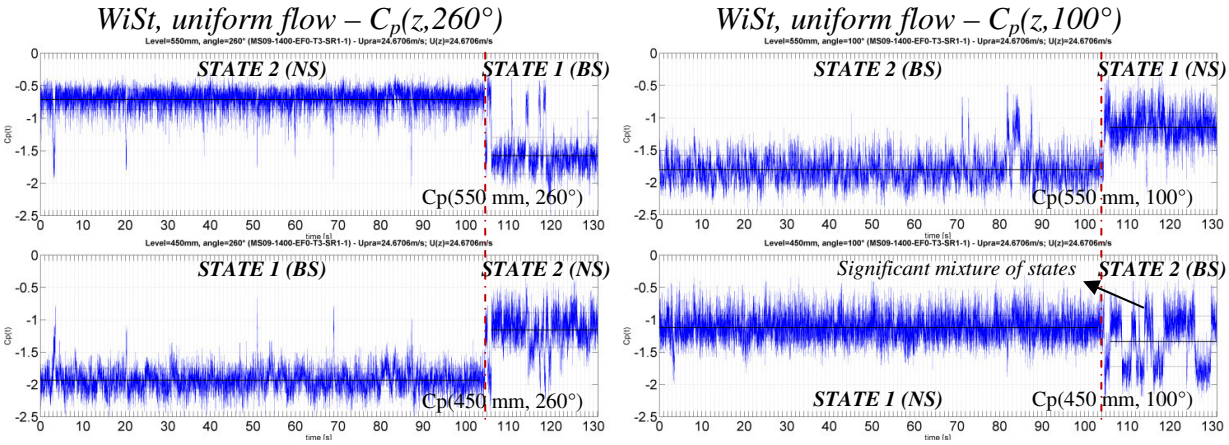

*Figure 6.13 Lowering of disruption level in uniform flow (WiSt, T3-SR1-EF0-R1, Re = 2.5*10^5)*

The inversion of the asymmetry along the height of the cylinder is confirmed at CRIACIV, as proved by the previous pictures. It is a sort of cascade effect, which is governed by the tip. Such a spanwise inversion is the result of an interaction between compartments. In order to motivate flow movements between compartments, the pressures and the pressure differences above and below one ring within only one state are plotted in Figure 6.14. The curves of $C_{p,m}$ at 910 and 890 mm are reported in the figure together with the green lines, namely Dp, which represent the difference $C_{p,m}(890) – C_{p,m}(910)$. At WiSt, on the side of the cylinder 0°-180°, the flow moves vertically towards the lower pressure, i.e. towards the compartment with the separation

bubble. This results, on the 0°-180° side of the cylinder, in a downwards movement. The opposite occurs on the other side of the cylinder, with an upwards movement, always towards the high-suction, i.e. the bubble-side. All of that is valid during each of the two stable states of the flow. In particular, in Figure 6.14 the results are averaged over the predominant interval. The results at CRIACIV are in wonderful agreement[5].

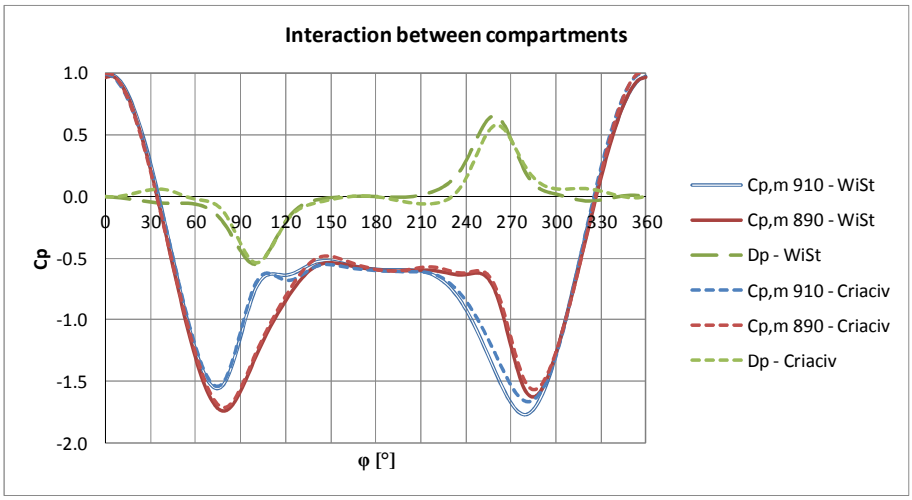

Figure 6.14 Pressures and pressure differences between compartments, above and below the ring n.9 (WiSt&CRIACIV, T1/T5-SR1-EF0-R1)

Figure 5.33 showed the cross-correlations of the lift coefficient at WiSt, with reference height z = 950 mm. In the case of ten rings, a drop of the cross-correlations at Δz = 100 mm due to the missing contribution of the tip-associated vortices was evident. Instead, such a contribution was not disturbed by the presence of only five rings. This is confirmed at CRIACIV in Figure 6.15, both in terms of cross-correlation coefficients and in terms of co-spectra.

In this regard, one comment deserves further attention. The results, so far, have shown:

- the asymmetric flow with spanwise inversion along the height is a cascade effect from the tip (see also section 6.4);
- although it seems to be a free-end effect, it is not merely governed by a modification of the top condition, i.e. by the top ring alone, because the bistable asymmetric flow disappears with five rings.. Rather, the phenomenon seems to be governed by the distribution of rings in the tip region. This conclusion would deserve to be further explored by experiments (Chapter 8).

[5] The predominant state at WiSt and Criaciv present separation bubbles on opposite sides. Therefore, in order to compare results in both wind tunnels within the predominant state, results at Criaciv are mirrored.

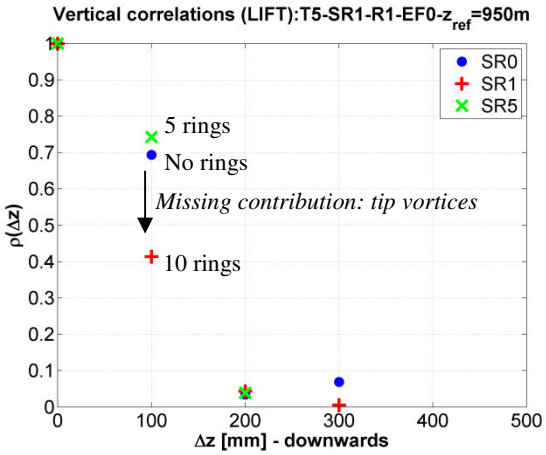

Figure 6.15 Cross-correlation coefficients of C_L without rings (blue), 10 rings (red) and 5 rings (green). z_{ref} = 950 mm. To be compared with Figure 5.33

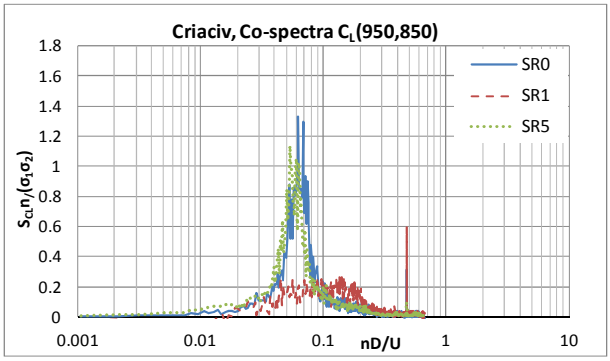

Figure 6.16 Co-spectra of C_L: $S_{CL}(z_1,z_2)*n/\sigma^2$ vs nD/U, z_1 = 950 mm, z_2 = 850 mm (CRIACIV, T5-SR0/SR1/SR5-EF0-R1). To be compared with Figure 5.34

6.3 Influence of the atmospheric boundary layer

The atmospheric boundary layer produces vertical velocity gradients which enhance the flow movement from regions of relatively high pressure to regions of relatively low pressure (Chapter 3). Because of that, differences between results in the two wind tunnels should be expected, even in the mean pressure and force coefficients. In addition, the fluctuating loads are related to the turbulence intensity of the flow and the different length scales influence the load correlation. Chapter 7 takes advantage of the tests in different conditions of the atmospheric boundary layer, in order to model the wind load with regard to the flow properties. In this section, the differences on the circular cylinder without rings are discussed at the beginning, the effect on the bistable flow is commented at the end.

As regards the mean pressure coefficients, the tests in the two wind tunnels on the circular cylinder without rings showed that the most significant differences occurred in the middle region of the tower. It should also be mentioned that below 600 mm in SR0 only 9 measurements per level (instead of 18) were available at CRIACIV. Fitting curves (splines) are used to interpolate data. The available measurements at CRIACIV are highlighted in the graphs in Figure 6.17. The graphs show that the tip effect is perfectly reproduced in the two wind tunnels, without significant influence of the different atmospheric boundary layer. In view of the investigation of the bistable asymmetric flow, this is a great advantage. Instead, lower suction in the wake, as well at the flanges, is apparent at CRIACIV e.g. at 450 mm (Figure 6.17c). The higher pressure at the flanges in CRIACIV may depend on the downstream movement of

spanwise flows, produced by the vertical pressure gradients. The mean suction in the wake is related to the steady recirculation region behind the tower and to the length of the eddy formation region. As shown in Chapter 3, the strength of the downwash in the near-wake may be weakened by the boundary layer. This issue is further addressed in the following with regard to the correlation coefficients.

In any case, the two wind tunnels agree in showing higher suction in the wake (and thus higher drag) close to the ground (see $C_{p,m}$ at 150 mm in Figure 6.17). The increase in the drag coefficient also in the lower half of the cylinder, and not only in the tip region was previously commented in Chapter 4, too, concerning preliminary results at WiSt.

Cp_σ is different in the two wind tunnels, due to different I_u. In particular, in Figure 6.17 at 950 mm Cp_σ at stagnation (directly related to I_u) is very small, much smaller than the fluctuations in the wake, which instead are almost the same in WiSt and CRIACIV. These latter are mainly body-induced. This issue, concerning body-induced and turbulence-induced pressure fluctuations, will be addressed in Chapter 7. The different values of Cp_σ (or, similarly, Cp_σ^2) in the two wind tunnels will be related to the corresponding turbulent intensities, in order to quantify the amount of body-induced fluctuations in laminar flow.

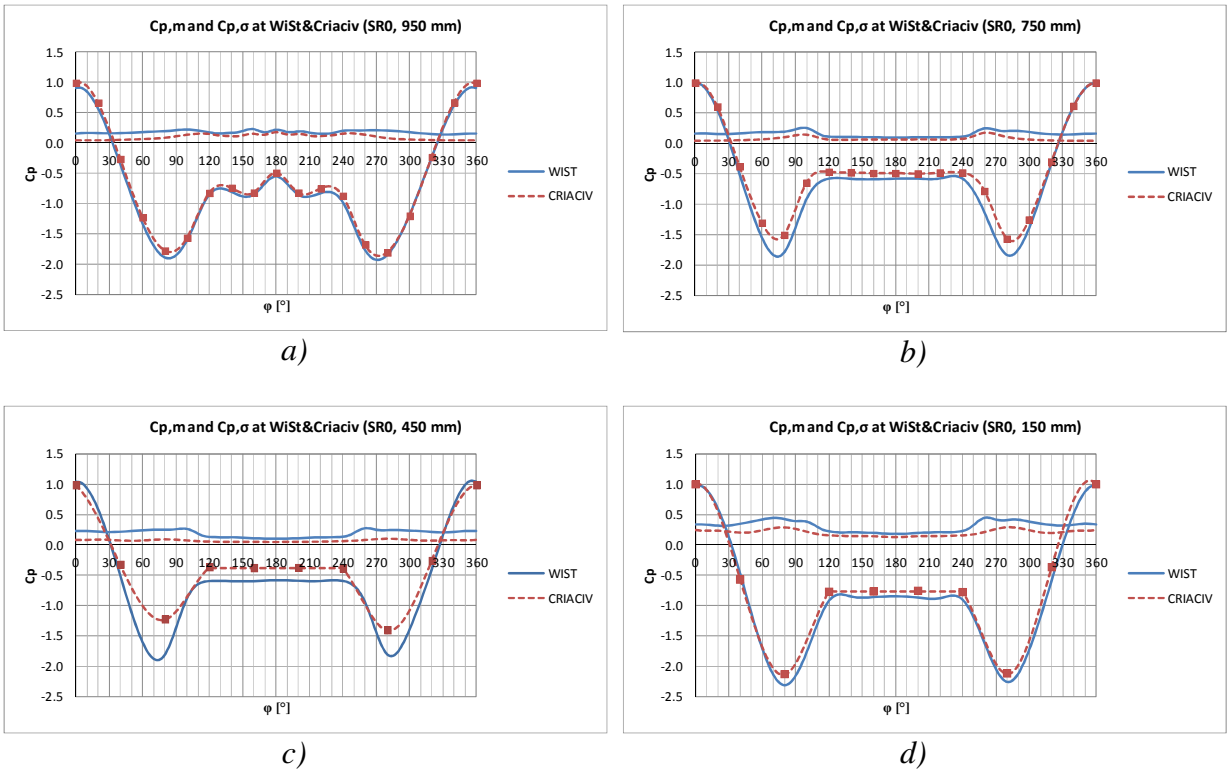

Figure 6.17 Mean and rms pressure coefficients at WiSt and CRIACIV (T1/T5-SR0-EF0-R1)

The cross-correlation coefficients and the correlation length L_{pz} depend on the correlation of the flow. In particular, L_{pz} can be related to L_{uz} (see Chapter 7). However, L_{uz} is not available at CRIACIV. In any case, the results at stagnation (where L_{pz} is directly related to L_{uz}) in the two wind tunnels do not show significant differences (Figure 6.18). L_{pz} at CRIACIV is generally lower, likely due to smaller L_{uz}.

The wake structure, instead, shows a certain dependency on the atmospheric boundary layer. As previously said, this is due to the strength of the downwash over the tip and to the formation of steady recirculation bubbles in the near-wake. The near-wake structure can be investigated by looking at the vertical cross-correlations. Representative graphs are shown in Figure 6.19, both in WiSt and in CRIACIV. Due to lack of data, the vertical cross-correlations at WiSt are measured at the angle 180°, while at CRIACIV the values at 160° are reported.

The cross-correlation $\rho(z_{ref}, \Delta z)$, with z_{ref} = 950 mm and Δz in the downward direction, shows that at WiSt there is a big steady vortex all along the height. Because of that, the cross-correlations are constant and different from zero even at large distance of separation. This cannot be modeled by a simple negative exponential function. The effect on the response will be quantified in Chapter 7, and it is now anticipated that it is not appreciably big (in the order of a few per cent of the response). In particular, the recirculation bubble at WiSt should arrive shortly above z = 50 mm (i.e. Δz = 900 mm). In CRIACIV, the same happens, but the recirculation bubble is smaller in size: it likely goes from the tip down to 450 mm. At larger distance of separation (Δz > 500 mm), the cross-correlation is zero. However, the steadiness of the recirculation bubble at CRIACIV is weaker, as shown by the rather low correlations even at small distance of separation, which weakly show a constant level.
In the lower half of the tower (z/H < 0.5), i.e. in the region of increase in the drag coefficient due to ground effects (see Chapter 4), a base vortex – maybe of the same type as that mentioned in Chapter 3 among the three-dimensional effects investigated by numerical simulations (Figure 3.18, Figure 3.19, Figure 3.20) – may be identified in the downwards cross-correlations with z_{ref} = 550 mm. The vortex can be identified by the still high correlation at Δz = 500 mm.
Last, but not least, it is interesting to observe that the upwards cross-correlations with z_{ref} = 50 mm show the same trend in the two wind tunnels. The base vortex is identified by the hump in the curve, at about Δz = 500 mm. At larger distances, the cross-correlations drop to zero.

WiSt *CRIACIV*

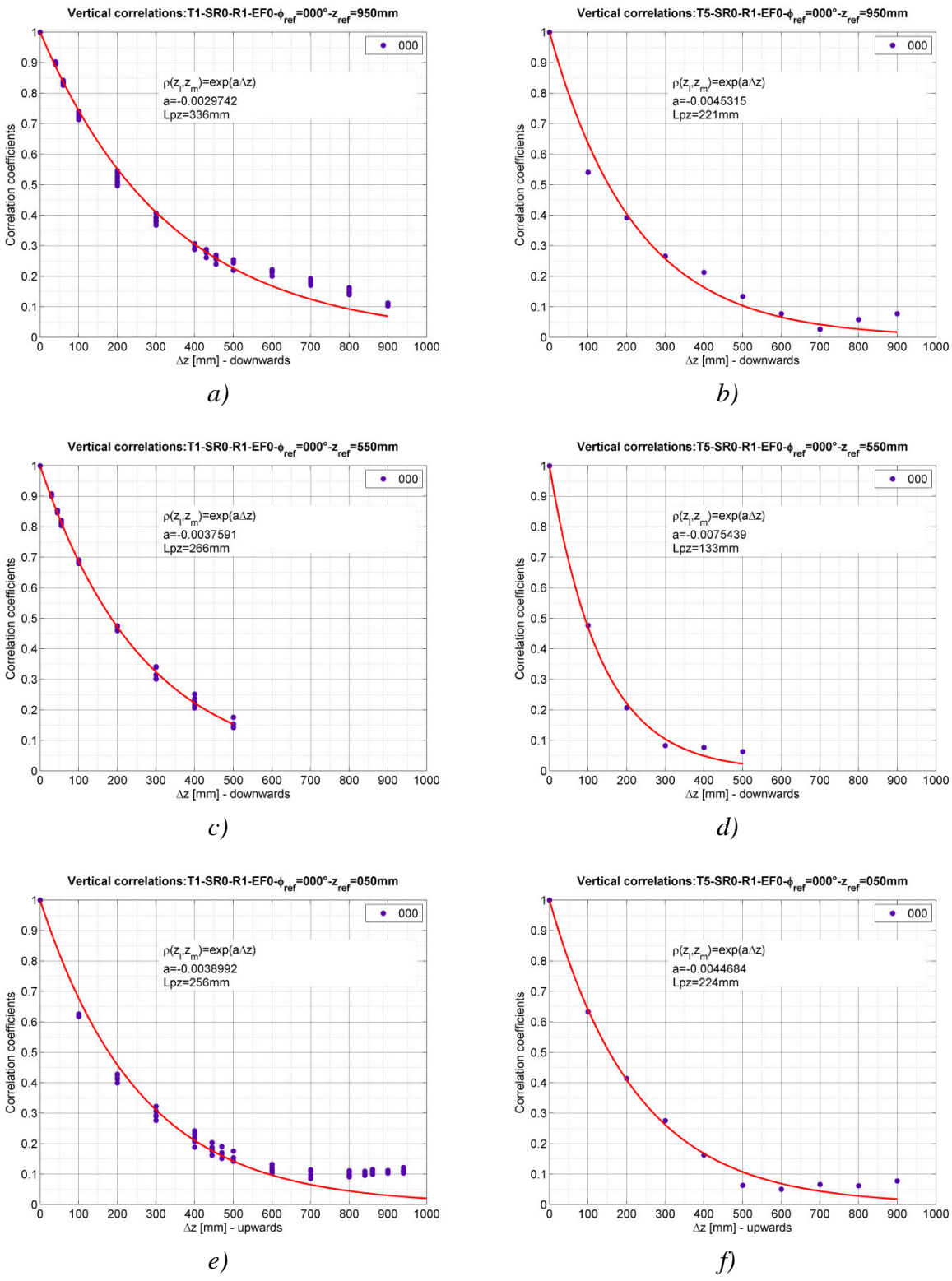

a) *b)*

c) *d)*

e) *f)*

Figure 6.18 Cross-correlation coefficients at stagnation, WiSt and CRIACIV (T1/T5-SR0-EF0-R1)

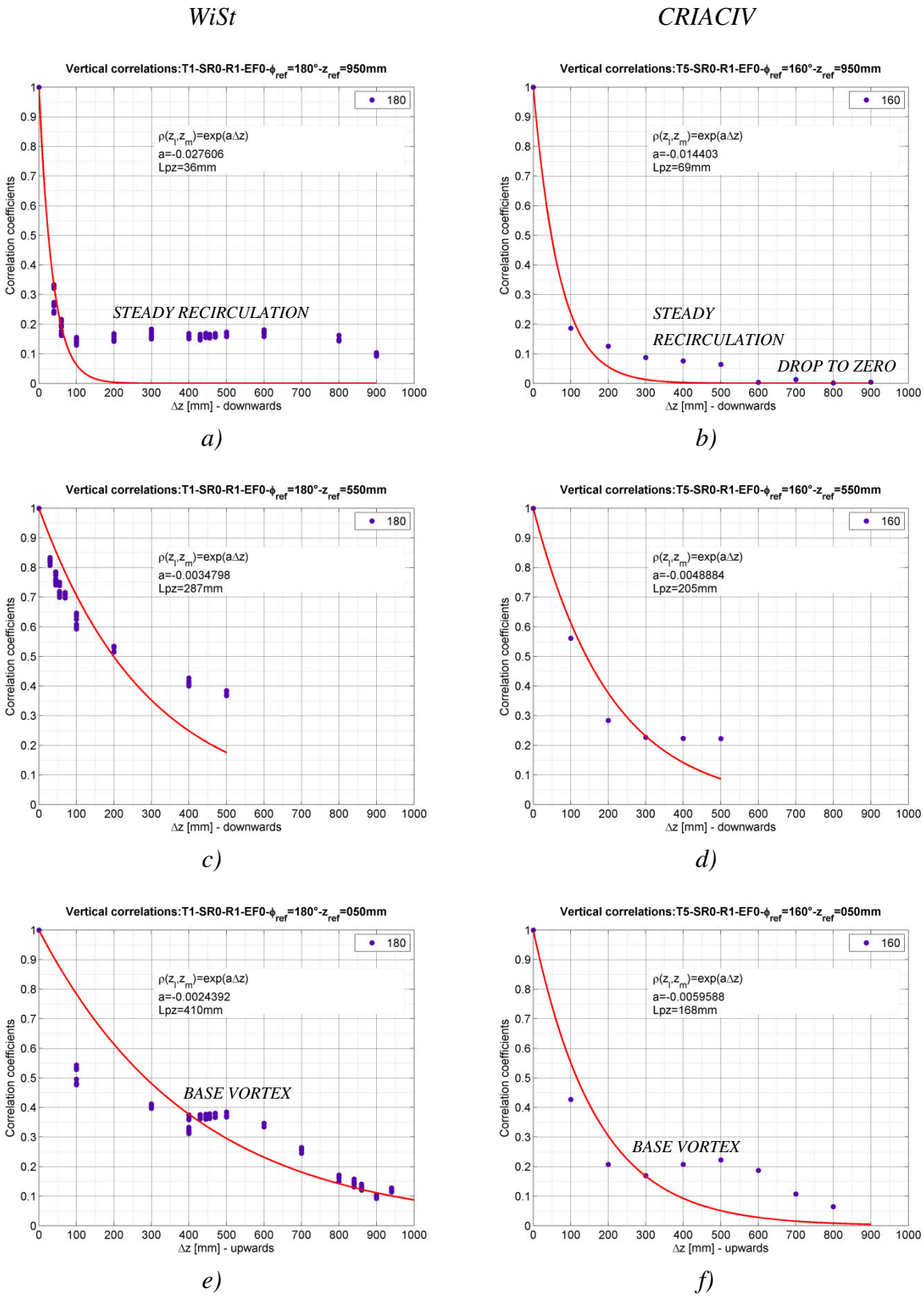

Figure 6.19 Cross-correlation coefficients in the wake, WiSt and CRIACIV (T1/T5-SR0-EF0-R1)

In the tip region of the cylinder, a low frequency peak – around one third of the Strouhal number – appears in the spectra due to the formation of tip-associated vortices.

As reported in literature (Kitagawa et al., 2001; Park&Lee, 2000), the shedding frequency of such big vortices is not deeply influenced by the boundary layer. The wind tunnel tests at CRIACIV, compared to those at WiSt, represent a further confirmation. However, the atmospheric boundary layer does influence the shedding along the height and the interaction between the low-frequency peak and the Karman vortex shedding. In particular, as proved by Figure 6.20, at WiSt the Karman vortex shedding ($S_t = 0.2$) strongly interacts with the tip-associated vortices already at $z/H = 0.85$ and definitely predominates at $z/H = 0.75$. All of that occurs at CRIACIV, too, but at a level which is lower of about 0.1H. In any case, it is confirmed in the spectra that in both wind tunnels the lower non-dimensional shedding frequency is about 0.065.

The explanation regarding the influence of the atmospheric boundary layer on the spanwise variation of the Strouhal number can be indirectly related to the different near-wake structure in the two wind tunnels (Figure 6.19). In fact, the decrease in the Strouhal number in the tip region is due to entrainment of flow over the tip (Farivar, 1981), as explained in the state of the art (Chapter 3). It is a sort of blockage effect, like a splitter plate, which elongates the eddy formation region. At CRIACIV, the atmospheric boundary layer is almost vanished in the tip region (i.e. the shear stress is almost null and the mean wind speed is constant). This can be a realistic situation, especially for the 1.5 km tower. In this condition, the effect is a stronger entrainment in the near-wake at high levels, as also confirmed by Park&Lee (2002) in uniform flow, with respect to boundary layer flow (Figure 3.31). So, at $z/H > 0.75$, the lower frequency peak predominates. Below such a level, the Karman vortex shedding peak arises. The almost constant noise at high frequencies in CRIACIV spectra, especially at $z/H = 0.65$, could be caused by the vibration of the turntable, which could not be completely avoided during the experiments.

It can be concluded that the near-wake structure is different in the two wind tunnels. Since the model is the same, such differences can only depend on the atmospheric boundary layer. In terms of mean wind load, this results in different wake suction (and thus different drag coefficient). In terms of fluctuating load, the spectra show a different interaction along the height between tip-associated vortices and Karman vortices.

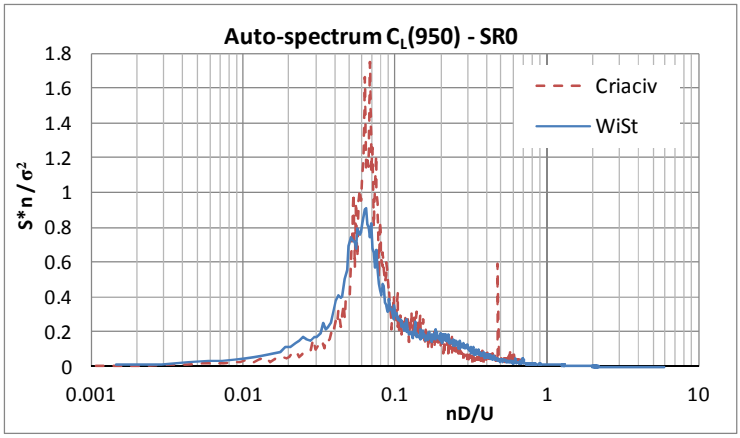

a) z = 950 m

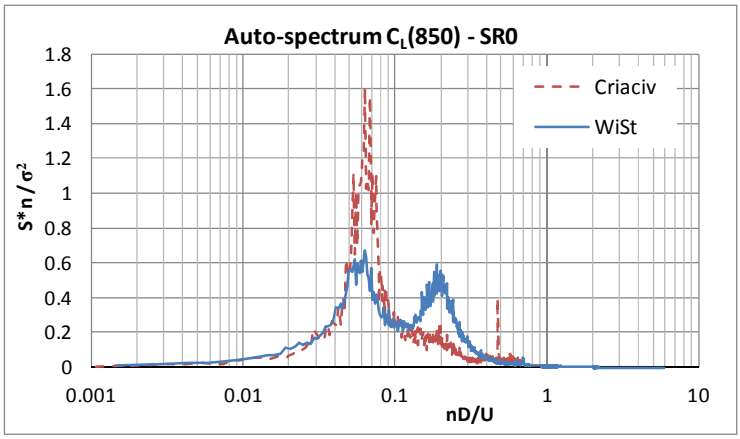

b) z = 850 m

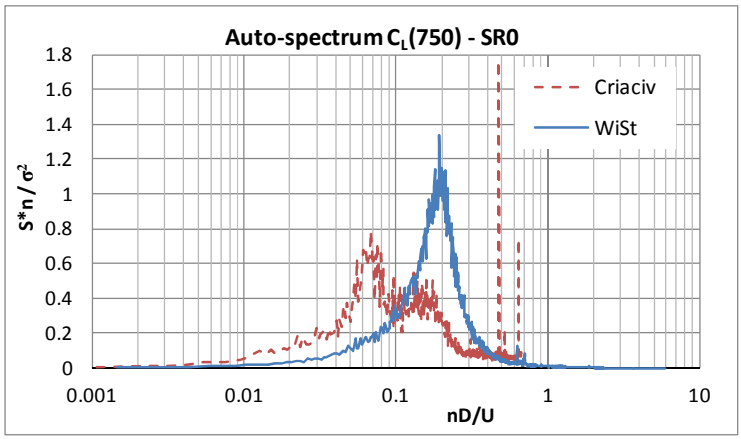

c) z = 750 m

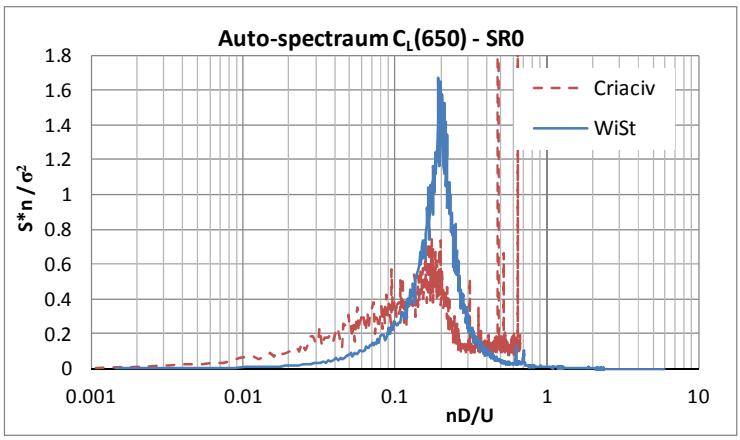

d) z = 650 m

Figure 6.20 a-d) Lift spectra along the height without rings at WiSt and CRIACIV (T1/T5-SR0-R1-EF0)

Last but not least, the atmospheric boundary layer has an influence on the vertical development of the bistable flow. It has been already anticipated that the disruption of the boundary layer starts higher at CRIACIV, with respect to WiSt (Figure 6.9). Unfortunately, measurements at low levels in case of 10 rings were not available at WiSt. They are instead available at CRIACIV and allow to define a complete overview along the height.

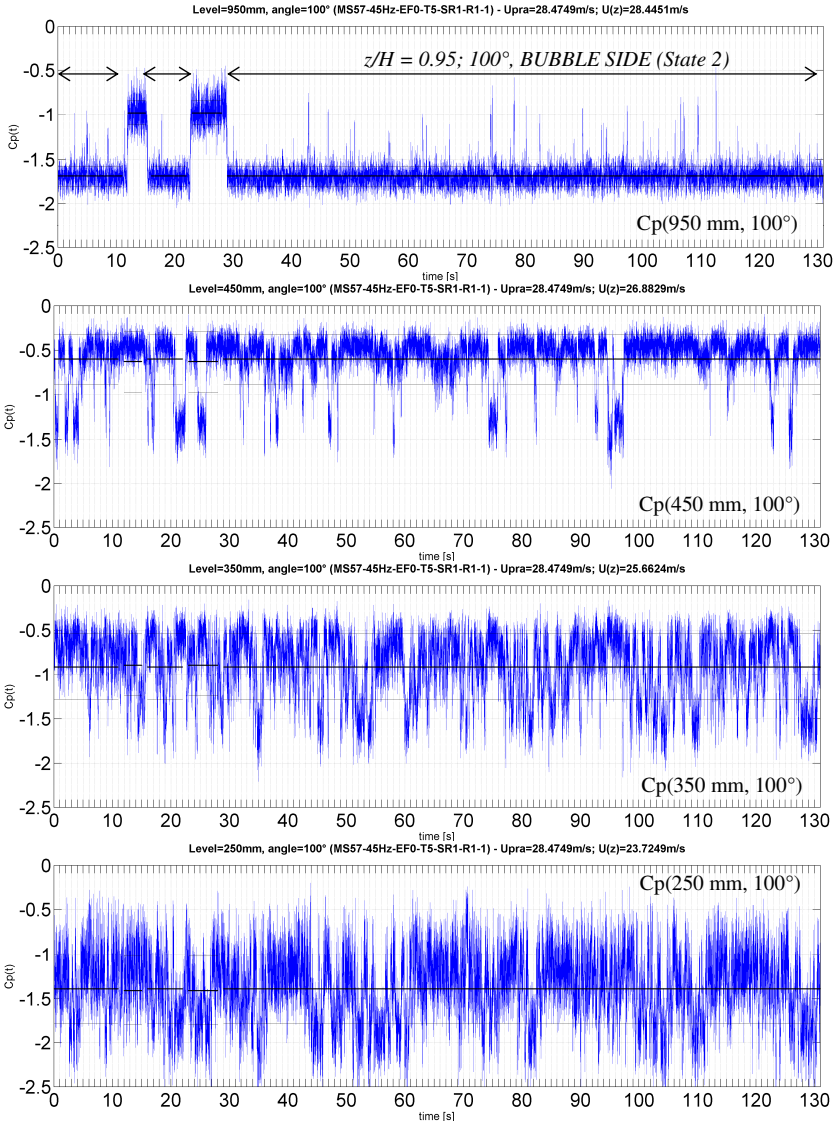

Figure 6.21 Bistability of the flow at low levels, $C_p(z/H,100°)$, simultaneous time histories (CRIACIV T5-SR1-R1-EF0, Re = $2.8*10^5$)

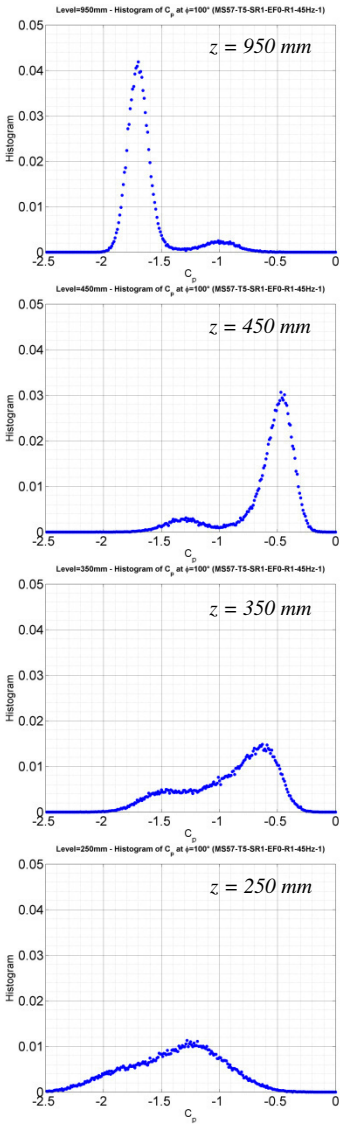

Figure 6.22 Bistability of the flow at low levels, histograms of $C_p(z/H,100°)$ (CRIACIV T5-SR1-R1-EF0)

The measurements along the height show that the flow is purely bistable and asymmetric only in the highest compartments (two at CRIACIV, three at WiSt). Here, bistable pressures produce bistable lift. Then, there is a region of transition (e.g. z =

650-750 mm in Figure 6.12, referring to CRIACIV data), where much more rapid jumps take place on the bubble side of the cylinder. The two states in the transition region are not well organized around the circumference, therefore they do not produce a purely bistable lift force. At lower levels ($z < 500$ mm, Figure 6.21) the time histories of pressures appear as an unstable sequence of states. In fact, the histograms of pressures on the right-hand side of the figure clarify that the pressures still oscillate between two states. Only closer to the ground (e.g. $z = 250$ mm in Figure 6.21), the bistability is substantially lost, not only in the lift but also in the pressures. The turbulence intensity certainly plays a role, although it is not the governing parameter of the bistable flow along the height.

6.4 Asymmetric bi-stable flow in CFD simulations

CFD simulations have been performed on the basis of CRIACIV experiments by the TEE group, Industrial Energy Dept. (formerly known as Energy Engineering Dept. "S. Stecco"), University of Florence (Salvadori&Mattana et al., 2013, unpublished personal communication).

The aim of the simulation is to provide numerical evidence of asymmetric bistable flow, as observed in the experiments. Therefore, the simulation refers to the most representative case: ten rings, no-efflux.

In the following, special attention is paid to those peculiar flow features which correspond to pressure characteristics observed in the experiments and commented up to now. However, the numerical study is only at the very first stage and it was not in the purpose of this work to proceed further. Further studies would be advisable in the future (Chapter 8).

The URANS simulation is performed by using the software Ansys Fluent 14. The incompressible fluid is solved by applying Navier-Stokes equations. The time step is 0.001 s, so about thirty time steps describe one period of vortex shedding. The turbulence model is the Shear Stress Transport (SST) k-ω. This is suitable to describe separated flows on smooth surfaces and adverse pressure gradients.

In order to reproduce the conditions of CRIACIV experiments, the tunnel and also the diffusor downstream of the test section were modelled. However, the presence of the diffusor is not relevant for the simulation and it can be ignored in further studies. Some pictures of the unstructured mesh are reported in Figure 6.23 and Figure 6.24.

The boundary conditions at the inlet are the velocity profile, the turbulence intensity and the turbulent length scale. The boundary conditions at the outlet are the pressure, the turbulence intensity and the turbulent length scale. No slip conditions are set to all

the other surfaces. The velocity profile at the inlet is like in Figure 6.2 (with maximum value equal to 28 m/s), while the turbulence intensity and the integral length scale L_{ux} are constant along the height, equal to 1% and 0.0075 m, respectively. These very low values will be increased in future studies, but may be representative in the tip region.

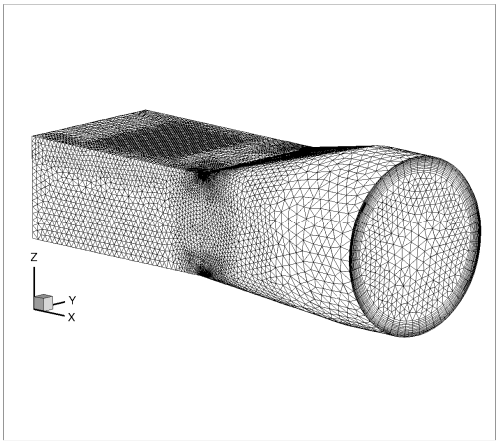

Figure 6.23 CRIACIV boundary layer wind tunnel – mesh (Salvadori&Mattana et al., 2013)

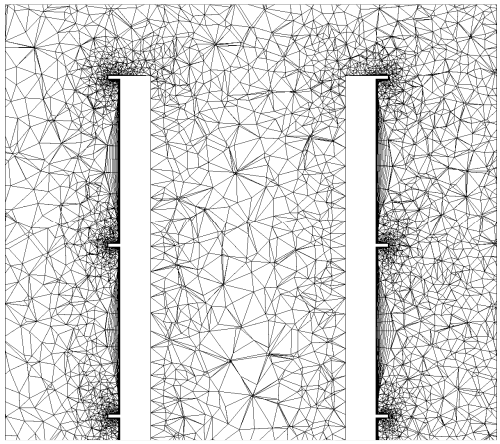

Figure 6.24 Detail of the mesh, transversal cross-section (Salvadori&Mattana et al., 2013)

A peculiar feature of the simulations is the high Re number (Re = $2.8*10^7$), obtained by reducing the air viscosity of two order of magnitudes ($\nu = 1.5*10^{-7}$ m^2/s). In these transcritical conditions of Re, surface roughness on the cylinder is not necessary. Moreover, differently from wind tunnel experiments, the simulation benefits of ideal test conditions.

The instantaneous flow picture in Figure 6.25 (horizontal cross-section at a representative level, 750 mm), clearly confirms the asymmetry due to a separation bubble on one side of the cylinder. This is consistent with the expectations on the flow, deduced on the only basis of pressure measurements in Figure 5.5 (WiSt) and Figure 6.10 (CRIACIV). The velocity magnitude shows the shift of the wake towards the bubble side. The streamline which separates on the normal side and reattaches on the bubble side motivates the high rms value on the bubble side in the wake. It is especially evident at about 200° in the state 1 (Figure 5.5/WiSt, Figure 6.10/CRIACIV).

Figure 6.26 plots the instantaneous vertical variation of the transversal velocity component, at the same time step as before. The cross-section cuts the cylinder in the across-wind direction Y at 120°-240° (X = 0.0375 m). The figure confirms the alternation between compartments (spanwise inversion), as observed in the experiments. The different colors in the figure on the two sides of the cylinder (i.e. blue on the right-hand side, standing for negative values and red on the left-hand side,

standing for positive values) are consistent with expectations: the transversal velocity vectors embrace the cylinder. In fact, what is interesting, and in agreement with the asymmetric phenomenon, is the different intensity of the transversal component on the two sides of the cylinder: in absolute value, the highest transversal velocity components are on the normal side. The differences in the transversal components on the two sides of the cylinder imply that the wake is not symmetrically aligned in each compartment, but it is shifted on one side. The same conclusion was also drawn from the experiments (Figure 5.40b).

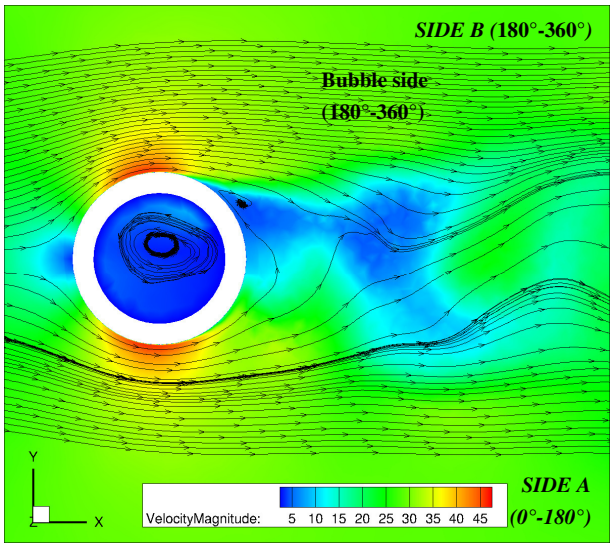

Figure 6.25 Horizontal cross-section, instantaneous flow velocity (magnitude, m/s) at z = 750 mm

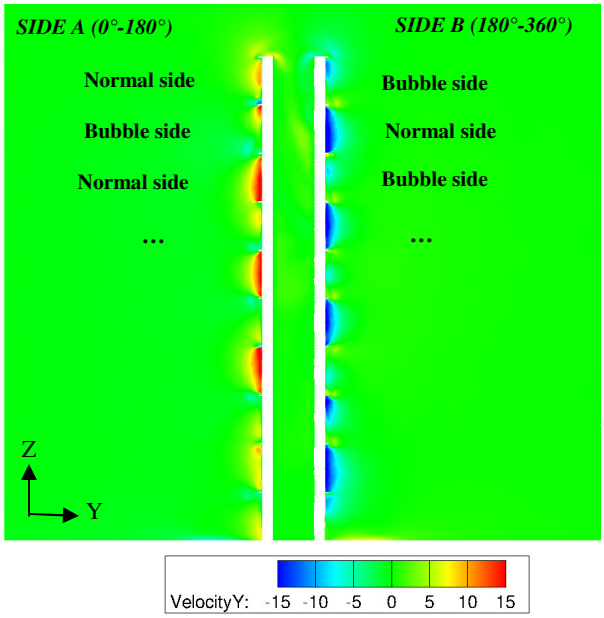

Figure 6.26 Transversal cross-sections, upstream view from the rear, instantaneous flow velocity (Y component, m/s) X = R/2 = 0.0375 m

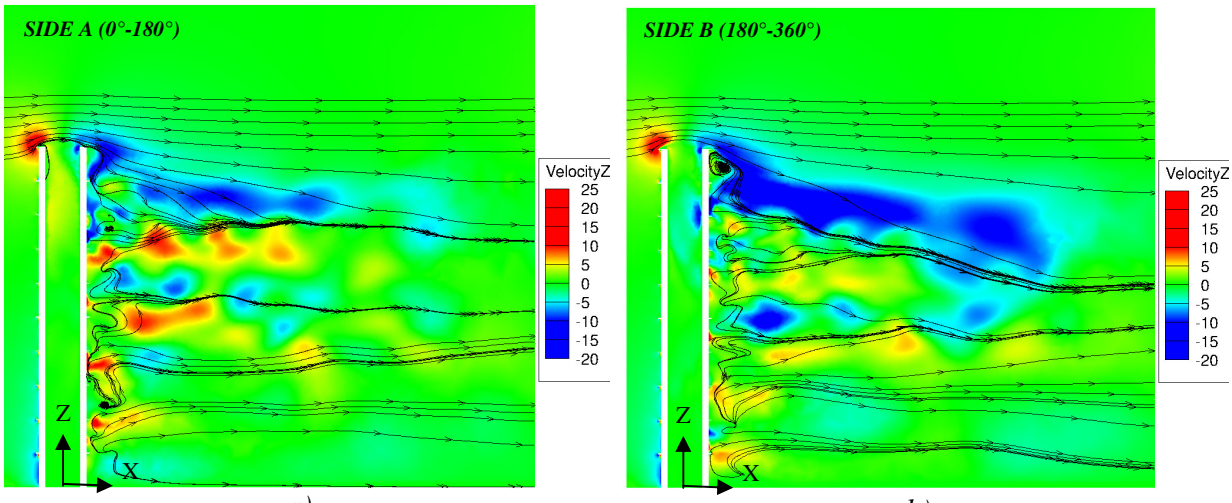

a) *b)*

Figure 6.27 Longitudinal cross-sections, instantaneous flow velocity (Z component, m/s) Y = +/- 0.0257 m (Salvadori&Mattana et al., 2013)

So far, the numerical simulation has provided evidence of the asymmetry around a symmetric structure, due to the formation of a separation bubble on one side of the cylinder. The other fundamental issue which characterizes the phenomenon is the bistability. In order to detect, during the simulation, whether a jump takes place at a certain level, several monitoring probes were placed in the wake of the cylinder. As shown by Figure 6.28, there are two probes on each level for ten levels. The level number 1 is 49 mm above the cylinder, the level number 2 is at the tower top and so on, with a distance between levels of 50 mm. In this way, the probes are placed at each level of the ring and in between two rings, until z/H = 0.6. The probes allow to monitor the absolute pressure during the simulation. It is clear from Figure 6.29, in particular at level 5 (z/H = 0.85), that a jump has taken place at about t = 0.2 s.

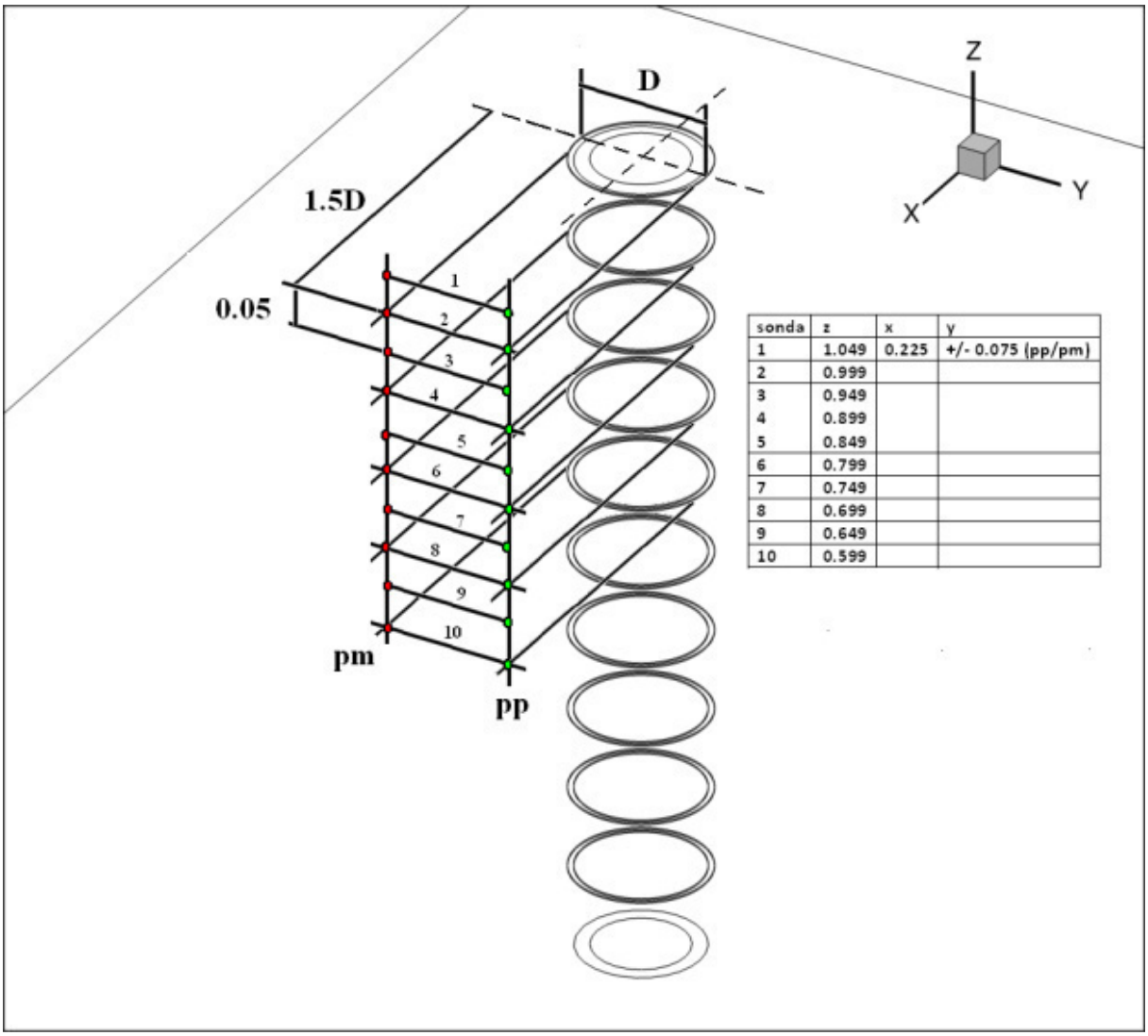

Figure 6.28 Sketch of the probes to monitor flow pressures in the wake (Salvadori&Mattana et al., 2013)

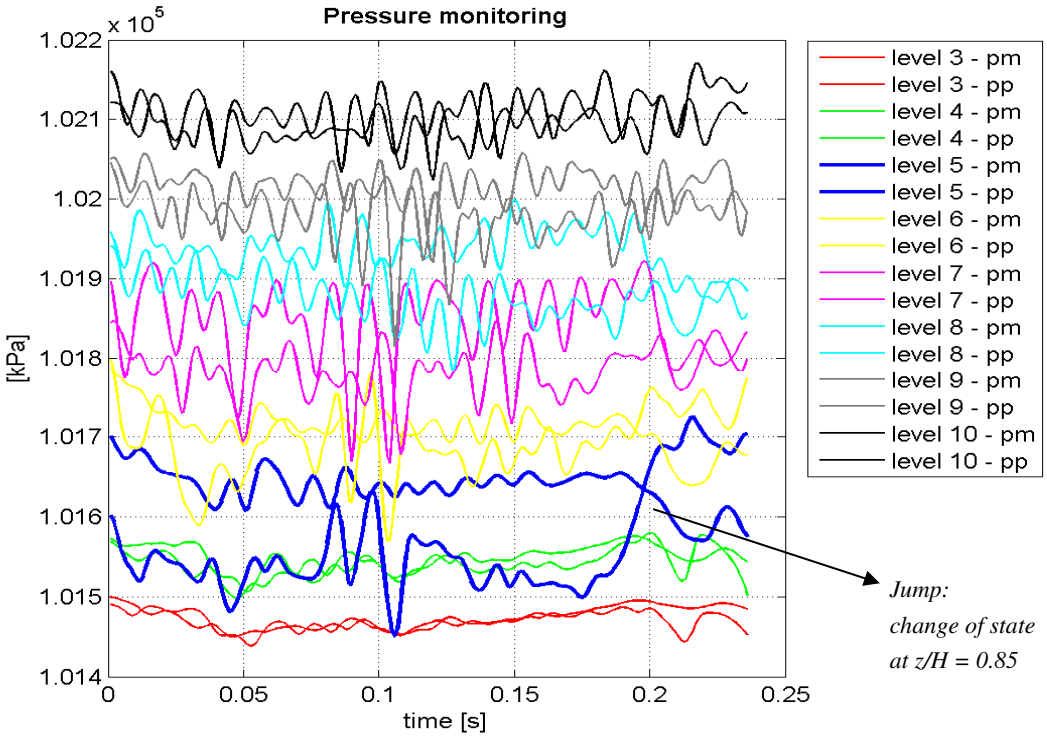

Figure 6.29 Time histories of flow pressures behind the tower (Salvadori&Mattana et al., 2013)

The most representative flow picture which highlights the occurrence of a change of state is the transversal cross-sections at a downstream distance of one radius from the tower in the along-wind direction. Figure 6.30 reports an instantaneous flow picture before a jump, Figure 6.31 reports an instantaneous flow picture once the transition of state is initiated in the tip region.

The simulation shows that the downwash over the tip of the cylinder – the green tongue diverting towards side B in Figure 6.30 and side A in Figure 6.31 – guides the asymmetric flow, with spanwise inversion along the height. Due to the veer of the downwash flow, the sort of "snake" in the wake of the cylinder starts to invert its shape. At the time step in Figure 6.31 (that is the last monitored time step in Figure 6.29), the "snake" keeps the same shape from the ground until about two compartments from the top. There, the transition of state has occurred, as proved by the blue lines at level 5 in Figure 6.29. In fact, the time window of the simulation is relatively short. The experiments provided much longer measurements. Therefore, it cannot be stated whether Figure 6.31 testifies an actual jump, or just an attempt of jump, which is not able to develop along the height. The simulation should then proceed further, but this goes beyond the purpose of this Dissertation and it will be object of future research (Chapter 8).

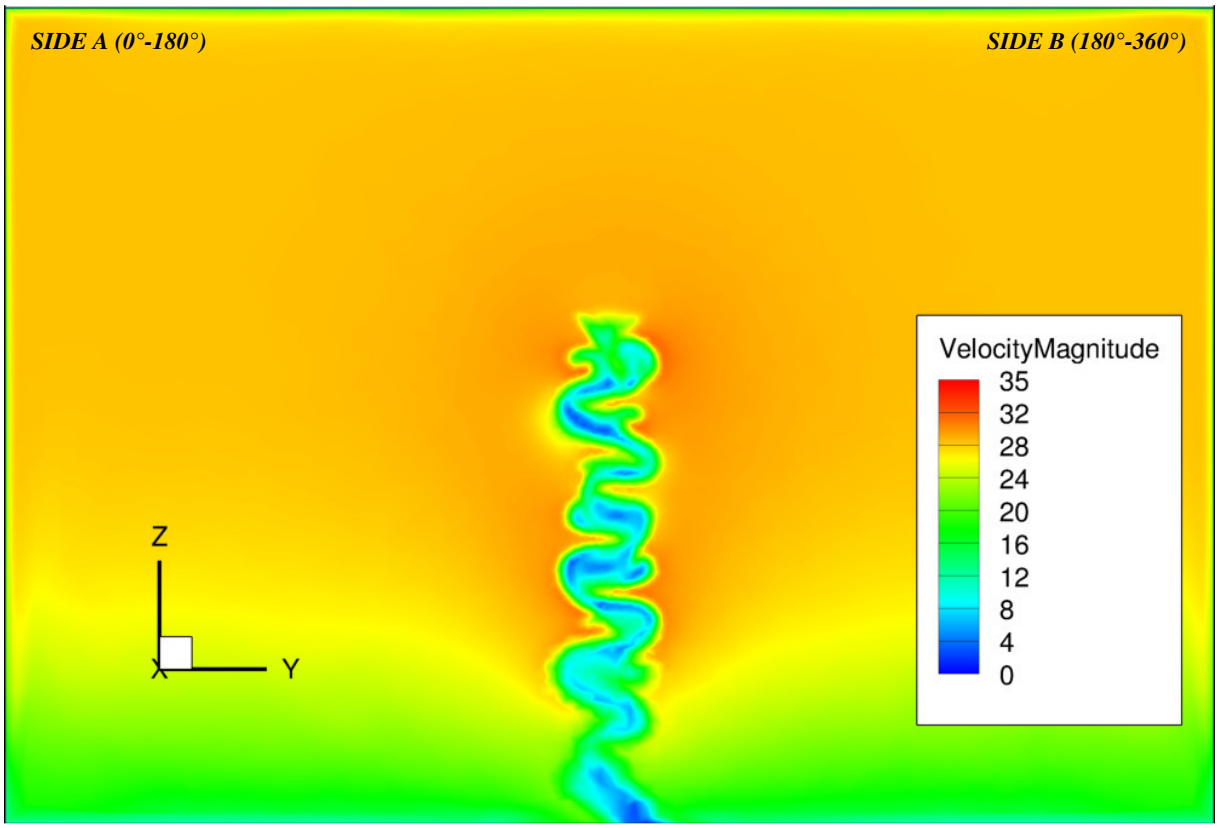

Figure 6.30 Transversal cross section in the wake at X = R from the tower (upstream view). Before the jump (t = 0). (Salvadori&Mattana et al., 2013)

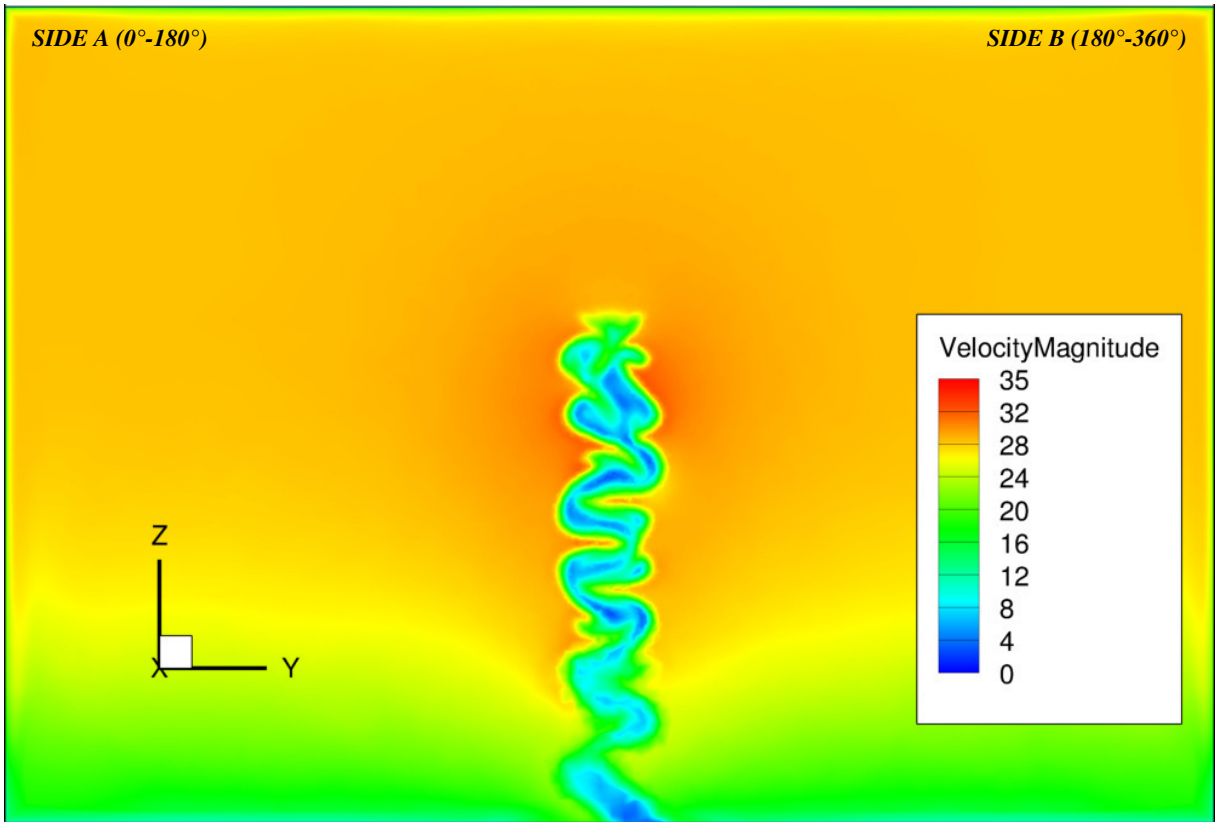

Figure 6.31 Transversal cross section in the wake at X = R from the tower (upstream view). After the jump (t = 0.024 s): transition of state is initiated in the tip region. (Salvadori&Mattana et al., 2013)

6.5 Concluding remarks

The experiments at WiSt and at CRIACIV aimed to discover, prove and understand a new asymmetric and bistable flow condition around circular cylinders, even at moderately high Reynolds numbers. The URANS numerical simulation supports the experimental evidence. However, the numerical study has been just introduced in the Dissertation; it will be the object of future research.

The question of the Reynolds number could not be fully addressed in the wind tunnel, but it had to be limited to the range of Re of the experiments, accompanied by surface roughness on the model. Moreover, experimental conditions in any laboratory are never ideal ones. The existence of any kind of disturbance or local flow distortion can promote asymmetric results. It is, in any case, very unlikely that two different laboratories promote the same asymmetric results due to their own test conditions. However, the cross-check of experiments could not fully answer the question of what would happen in ideal test conditions. This question cannot be addressed experimentally anyhow. From this point of view, the CFD provides the most reliable answer. The proof of existence of an asymmetric effect on a symmetric structure in symmetric flow condition is one of the most important contributions of the CFD simulation. A further contribution is, of course, the occurrence of the jump. Further studies are now necessary to investigate the occurrence of jumps. What can be stated now, is that the occurrence of asymmetric and bistable condition is not a matter of the Re. Moreover, from the experiments it is clear that the stable condition in the highest compartments in the case of ten rings is the asymmetric one, on either side of the cylinder. The CFD is presently too short to confirm the same result. This is an issue which would deserve further attention in the future, especially with regard to the effect of the Reynolds number and ideal test conditions.

The CFD clarified a peculiar feature, also observed in the experiments: the formation of a separation bubble on one side of the cylinder and the misalignment of the wake between different compartments. This is due to the cross-wind component, which predominates on the normal side of the cylinder and diverts the wake towards the bubble side. In particular, the cross-wind component predominates on the side of the cylinder where the vertical downwash is weaker (i.e. on the normal side). This would confirm the key role of the flow over the tip of the cylinder, whose downwash is mainly reversed on the bubble side, where it creates a secondary vortex below the highest ring. For this reason, the presence of efflux inside the cylinder cancels the

asymmetric phenomenon. In fact, the downwash flow over the tip is disturbed by the upwards flow out of the tip. It can be then wondered whether it is possible to identify a critical ratio between the Reynolds number of the incoming flow and the Reynolds number of the efflux, which is able to suppress the phenomenon.

Along the height, strips of flow cross each other in neighboring compartments and are responsible for the spanwise inversion. It is reasonable that all these flow movements kill the shedding of tip-associated-vortices. In fact, the lower shedding frequency is due to entrainment in the wake. This is, in case of rings, displaced on either side of the cylinder.

It should also be remembered that the formation of asymmetric separation bubbles disappears if the rings are at a sufficiently large distance (experimental evidence only, CFD not performed). With regard to that, Figure 6.27 shows the effect of ring n.9 (z/H = 0.9) in constraining the recirculation vortex within the highest compartment. Therefore, the role of ring n.9 in the whole phenomenon should be further investigated.

The experimental and numerical evidence of the new phenomenon proposed in this Dissertation is now fully confirmed. It opens the doors to the last step of this work, that is the evaluation of load and response (Chapter 7). In this regard, it is important not to restrict the analysis to the interesting but unique design condition of ten rings along the height. Because of that, the study of the load and the response of the tower is addressed in a wider perspective. But of course, the response to the asymmetric and bistable flow needs to be quantified, too.